

ARTICLE OPEN

Electron–phonon coupling in superconducting 1T-PdTe₂

Gloria Anemone^{1,2,3}✉, Pablo Casado Aguilar^{1,2}, Manuela Garnica², Fabian Calleja², Amjad Al Taleb², Chia-Nung Kuo⁴, Chin Shan Lue⁴, Antonio Politano^{5,6}, Amadeo L. Vázquez de Parga^{1,2,7,8}, Giorgio Benedek^{9,10}, Daniel Farías^{1,7,8} and Rodolfo Miranda^{1,2,7,8}

We have determined the electron–phonon interaction in type II Dirac semimetallic 1T-PdTe₂ by means of helium atom scattering. While 1T-PdTe₂ is isostructural with 1T-PtTe₂, only the former is superconductor. The difference can be traced to the substantially larger value of the electron–phonon coupling in 1T-PdTe₂, $\lambda = 0.58$, obtained from the Debye-Waller attenuation of the He specular peak. With this value and the surface Debye temperature, $\Theta_D = 106.2$ K, we have figured out the superconducting critical temperature, $T_c = 1.83$ K given by the BCS theory, which is in good agreement with $T_c = (1.95 \pm 0.03)$ K obtained with low-temperature scanning tunneling microscopy. The value of the effective mass related to Θ_D indicates that the large electron–phonon coupling in 1T-PdTe₂ is due to coupling, not only with the zone-center optical mode O_2 at 9.2 meV, as proposed in a recent theoretical study, but also with the zone-boundary acoustic mode LA. Our results suggest that the topological states of a Dirac cone play a negligible role on the onset of superconductivity.

npj 2D Materials and Applications (2021)5:25; <https://doi.org/10.1038/s41699-021-00204-5>

INTRODUCTION

In the last years, the 2D transition-metal dichalcogenides (TMDs) of general formula MX_2 , where M is a transition metal from group 4 to 10 and X is a chalcogen, have received significant attention due to their intriguing electronic and optical properties varying from topological Dirac semimetals to semiconductors, which turn them potentially useful in a wide range of applications^{1–6}. 1T-PdTe₂, in particular, presents a unique property: the coexistence of superconductivity^{7–10} with a type-II Dirac semimetallic phase¹¹. It was after the discovery of the topological properties of the isostructural, non-superconducting 1T-PtTe₂ crystal, when the interest in 1T-PdTe₂ grew rapidly. Even though an unconventional origin of the superconductivity in 1T-PdTe₂ was dismissed^{8,12}, type I, type II, and mixed-phase superconducting behaviors with multiple critical fields (H_c) were reported^{13–15}. However, the relevance of topological states of Dirac cone for the appearance of superconductivity is still under debate. In a more recent work, a different mechanism has been suggested, namely that superconductivity in 1T-PdTe₂ is triggered by an increase of the electron–phonon (e-ph) coupling constant λ , which is the consequence of a van Hove singularity at the Fermi level⁹.

The focus of the current study is the experimental determination of the e-ph coupling constant λ of 1T-PdTe₂ using helium atom scattering (HAS) and the correlation of these results with the superconductor transition temperature measured by low-temperature scanning tunneling microscopy (LT-STM). HAS is a well-established tool to investigate the structure and the dynamics of the outermost surface layer of any material in a completely nondestructive manner¹⁶. Recent theoretical studies showed how the thermal attenuation of the He specular peak from metal surfaces, described by the Debye-Waller exponent, can be directly related to the mass enhancement factor, i.e., the e-ph

coupling constant λ ^{17–19}. This approach has been recently adapted to derive λ for the case of degenerated semiconductors and chalcogenides^{20,21}.

We determined with HAS the frequency of the phonon modes which make a larger contribution to λ in 1T-PdTe₂ with respect to the isostructural 1T-PtTe₂. The frequency obtained is consistent with the mechanism for superconductivity proposed recently by Kim et al.⁹ for PdTe₂, in which electrons at a van Hove singularity near the Fermi level interact strongly with Te phonon modes. In addition, we found that a large contribution to λ comes from the longitudinal acoustic (LA) mode at the zone boundary, which suggests that the topological states of a single cone play a negligible role on the onset of superconductivity. Finally, STM results of the temperature dependence of the superconducting gap show that 1T-PdTe₂ is a medium-coupling conventional BCS superconductor in accordance to the value found for λ .

RESULTS AND DISCUSSION

Surface structure of PdTe₂ by HAS

1T-PdTe₂ crystallizes in the CdI₂ structure with space group $P\bar{3}m1$, as shown in Fig. 1a, b. The structure consists of one layer of hexagonally arranged Pd atoms sandwiched between two layers of Te atoms, forming a trilayer (TL). Adjacent trilayers are held together by weak van der Waals forces, which allows for easy exfoliation. The X-ray diffraction (XRD) measurements of the crushed crystals yield values of in-plane, $a = b = 4.0387$ Å, and out-of-plane, $c = 5.1361$ Å, lattice parameters (see Supplementary Figs. 1 and 2), in agreement with previous crystallographic neutron values, $a = b = 4.0365$ Å and $c = 5.1262$ Å²². Figure 1c shows in-plane (blue curve) and out-of-plane (orange curve) angular distributions of He atoms scattered from the PdTe₂

¹Departamento de Física de la Materia Condensada, Universidad Autónoma de Madrid, Madrid, Spain. ²Instituto Madrileño de Estudios Avanzados en Nanociencia (IMDEA-Nanociencia), Madrid, Spain. ³Departamento de Matemática Aplicada y Estadística, Universidad San Pablo-CEU, CEU Universities, Madrid, Spain. ⁴Department of Physics, National Cheng Kung University, Tainan, Taiwan. ⁵Dipartimento di Scienze Fisiche e Chimiche (DSFC), Università degli Studi dell'Aquila, L'Aquila, Italy. ⁶CNR-IMM Istituto per la Microelettronica e Microsistemi, Catania, Italy. ⁷Instituto 'Nicolás Cabrera', Universidad Autónoma de Madrid, Madrid, Spain. ⁸Condensed Matter Physics Center (IFIMAC), Universidad Autónoma de Madrid, Madrid, Spain. ⁹Dipartimento di Scienza dei Materiali, Università di Milano-Bicocca, Milano, Italy. ¹⁰Donostia International Physics Center (DIPC), University of the Basque Country (EHU-UPV), Donostia/San Sebastián, Spain. ✉email: gloria.anemone@gmail.com

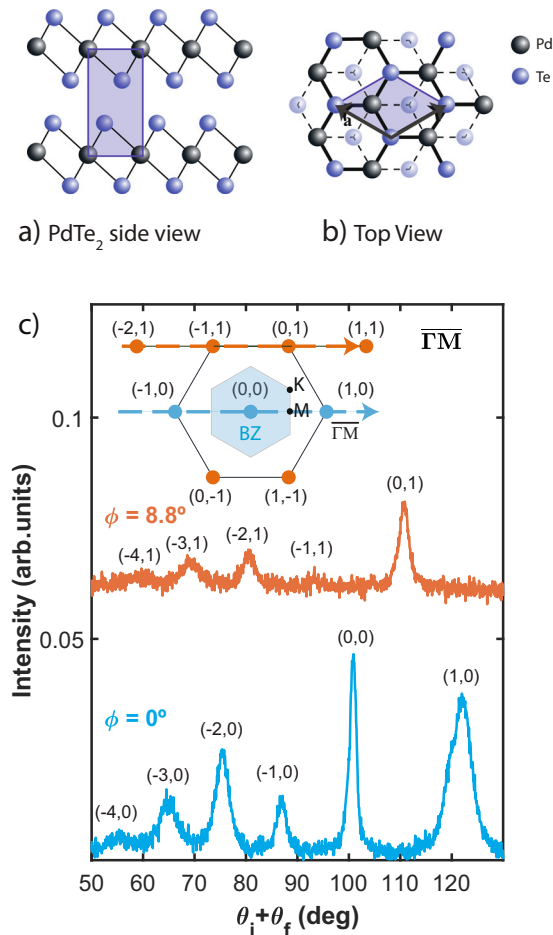


Fig. 1 Structural characterization of PdTe₂ by HAS. **a** Side and **b** top views of the PdTe₂ crystal structure. **c** In-plane and out-of-plane (blue and orange curves, respectively) He diffraction spectra from 1T-PdTe₂ along $\bar{\Gamma M}$ measured with an incident angle of 50°. The incident energy is $E_i = 49.5$ meV and the surface temperature is $T = 90$ K. The inset in (c) shows the PdTe₂ lattice in reciprocal space. Orange and blue colored spots are diffraction peaks, and blue shaded area is the Brillouin zone (BZ).

surface, measured along $\bar{\Gamma M}$. The crystallinity and the high-quality of the surface is demonstrated by the observation of the diffraction peaks up to the third order, both in-plane and out-of-plane. As can be seen in Fig. 1c even the fourth-order diffraction peak $(-4, 0)$ is clearly resolved. Among the in-plane diffraction peaks, the specular peak $(0, 0)$ presents the highest intensity, with an absolute reflectivity (normalized with respect to the incident He beam) of $\sim 0.7\%$. Note that the diffraction peak $(-1, 0)$ has a lower intensity than the second diffraction peak $(-2, 0)$, due to the surface corrugation. The total reflectivity of the sample surface (including the two symmetric out-of-plane diffraction patterns) amounts to $\sim 7\%$. By analyzing in-plane and out-of-plane angular distributions taken at different incident conditions we have determined the in-plane lattice constant as $a = (3.95 \pm 0.05)$ Å, which is similar to the value obtained in earlier X-ray studies^{23,24} and almost identical to the one of 1T-PtTe₂, reported elsewhere²⁵. From the evolution of the specular intensity as a function of incident angle (see Supplementary Note 2 and Supplementary Fig. 3 for more details), the interlayer spacing, i.e., the step height observed ($d = 5.12 \pm 0.05$ Å) is in excellent agreement with neutron data²². This means that mechanical exfoliation of PdTe₂ leads mainly to the appearance of single trilayer steps.

Surface structure of PdTe₂ by STM

STM images taken at 1.25 K reveal a flat surface as illustrated in Fig. 2a. The line profile (Fig. 2c) measured along the white line in Fig. 2a shows a step height of $h = (5.0 \pm 0.2)$ Å (see also Supplementary Note 3 and Supplementary Fig. 4), consistent with the bulk value obtained by XRD ($c = 5.1361$ Å) and HAS measurements. This corroborates that the steps are single trilayer-high. As can be seen in the atomically resolved image reproduced in Fig. 2b and the corresponding profile (Fig. 2d), only the Te atoms of the last layer are observed with an apparent corrugation of 0.08 Å at these particular set-point conditions. Topographic STM images taken with different set point conditions and tips show a change in the corrugation, see Supplementary Fig. 5. In defect-free areas, the Te atoms form a triangular structure with an in-plane lattice constant of $a = (4.03 \pm 0.11)$ Å, in agreement with the HAS measurements described above and with previous XRD and STM data^{26–29} and with the one extracted from our own XRD measurement ($a = 4.0387$ Å) shown in Supplementary Fig. 2. The 3D characters of the topological states at the Fermi surface and of the electron–phonon interaction (see below) result in the structural similarity of the surface trilayer (TL) with the bulk TLs.

Characterization of superconducting gap by STS

Figure 3a shows the local differential conductance (dI/dV) of the 1T-PdTe₂ surface measured at 1.25 K without an applied magnetic field, which allows to resolve the coherence peaks and a well defined superconducting gap. The value of the energy gap resulting from the Bardeen, Cooper, and Schrieffer (BCS) theory fit at 1.25 K is $\Delta = 0.43$ meV (see Supplementary Note 4 for more details). In order to characterize the 1T-PdTe₂ superconducting properties, a series of differential conductance spectra were recorded as a function of temperature and perpendicular magnetic field. Figure 3c shows the evolution of the SC gap as a function of the temperature, revealing a critical temperature slightly below 2 K. The corresponding Δ values are very well fitted by a simplified version of the formula for a medium-coupling BCS superconductor³⁰, $\Delta(T) = \Delta(0) \tanh[\frac{1}{2} \pi (T_c/T - 1)^{1/2}]$, with the required mean-field critical exponent 1/2 for $T \rightarrow T_c$. The resulting critical temperature is $T_c = (1.95 \pm 0.03)$ K, in agreement with Xiao et al.³¹ and Kim et al.⁹ calculations for zero pressure ($T_c = 1.95$ K and 1.79 K, respectively) and Das et al.⁸ STS measurements (1.78 K). The present value is however larger than those from resistivity (1.64 K)^{13,32} or AC-susceptibility measurements at ambient pressure (1.60 K)³³, as well as at the onset of surface superconductivity ($T_c^s = 1.52$ K³³). The corresponding value of the ratio $\Delta(0)/k_B T_c = 2.93$ is larger than the BCS weak-coupling ratio (1.764). The evolution of the SC gap with the temperature and the ratio between the gap and the critical temperature indicate that 1T-PdTe₂ is a medium-coupling conventional BCS superconductor.

The evolution of the SC gap at 1.25 K with a perpendicular magnetic field increasing from 0 to 2.1 T is reproduced in Supplementary Fig. 6 (see also Supplementary Note 5). The critical magnetic field at this temperature is around 2.20 T, which is within the wide range of values reported before^{12,15}.

Electron–phonon coupling constant determination

The thermal attenuation of the He specular peak for 1T-PdTe₂ measured with different incident energies and angles (red and blue diamonds) as a function of temperature is shown in Fig. 4. Similar data have been reported for the isostructural 1T-PtTe₂²⁵. The data can be described by the Debye–Waller model¹⁶, which takes into account the effect of the thermal vibrations of the surface atoms on the intensity of all quantum scattering features (diffraction peaks, specular elastic, and inelastic scattering). The Debye–Waller (DW) factor relates the intensity $I(T)$ of the specular

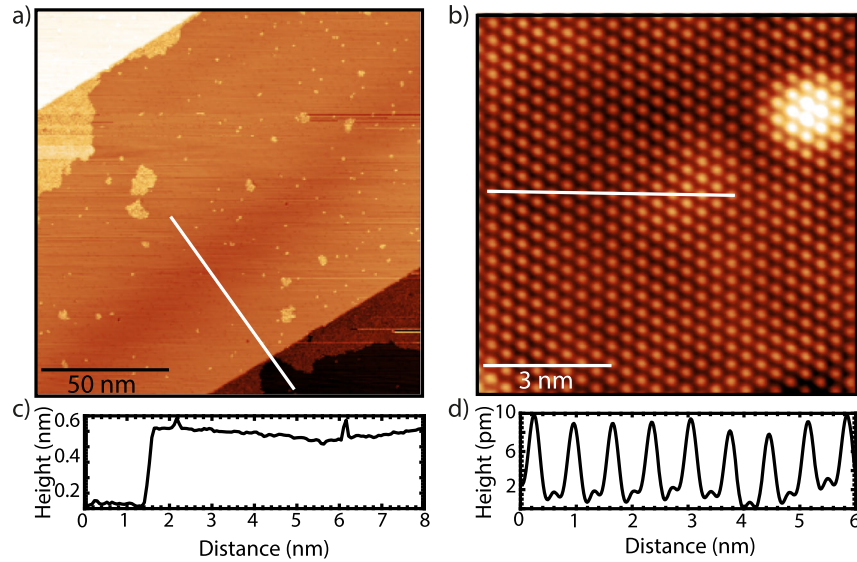


Fig. 2 STM images of PdTe₂. **a** Large scale STM topographic image of the 1T-PdTe₂ surface ($V_t = 1$, $V_i = 50$ pA); **b** Atomically resolved STM image ($V_t = 40$ mV, $I_t = 1$ nA). Both STM images were taken at 1.25 K; **c** Line profile taken along the line in **(a)**; **d** Topographic modulation along the line profile following the white line in **(b)**.

peak to the intensity I_0 reflected from a lattice at rest by:

$$I(T) = I_0 e^{-2W(T)} \quad (1)$$

where $2W(T)$ is the Debye–Waller exponent.

The 1T-PdTe₂ layered semimetal crystal can be viewed as a stack of two-dimensional electron gases in each TL, with n_s being a number of parallel TLs whose phonon displacements produces some modulation of the surface electronic density probed by the He atoms. For a conducting surface, the HAS DW exponent for specular reflection has been shown¹⁹ to be directly related to the e-ph coupling strength λ through the equation

$$\lambda = \frac{\pi\phi}{n_s a_c k_{iz}^2} \frac{\partial W(T)}{k_B \partial T} \quad (2)$$

where $\phi = 4.6$ eV³⁴ is the work function, $a_c = 14.1$ Å², the surface unit cell area, k_{iz} the normal component of the incident He atom wavevector and k_B the Boltzmann constant. The dependence of the DW exponent with T is obtained from the experiment and all other factors (except n_s) are known. In order to estimate n_s we rely on the detailed experimental (ARPES) and theoretical analysis by Bahramy et al.³⁵, which indicates that PdTe₂ is a topological material with a bulk Dirac point located at ≈ 0.5 eV below the Fermi level and $k_z \approx 0.85\pi c_0$ on the surface BZ center. The topological surface state is confined within a few surfaces TLs. The calculated electronic DOS projected on single orbitals and TL pairs show no significant surface features beyond the second TL. Thus, $n_s \approx 2$ is appropriate for 1T-PdTe₂, similarly to the values used for other TM chalcogenides^{21,25} (see Supplementary Note 6 and Supplementary Discussion). With $n_s = 2$, the linear fit of $-2W(T)$ in Fig. 4 and the above input data, Eq. (2) yields $\lambda = 0.58 \pm 0.03$ (See Supplementary Note 7), in excellent agreement with the theoretical $\lambda = 0.53$ ⁹. The larger value of λ found for 1T-PdTe₂ in comparison with the isostructural 1T-PtTe₂ ($\lambda = 0.38$ ²⁵) is consistent with the difference in the phonon dispersion modes for these two materials. As suggested by Kim et al.⁹, the van Hove singularity (vHs) in the electronic states is responsible for the stronger electron–phonon coupling in 1T-PdTe₂, with a consequent larger contribution to its superconductivity.

According to McMillan formula valid for BCS superconductors^{36,37}, the transition temperature, T_c , can be determined from a temperature, Θ , corresponding to an average phonon frequency weighted by e–ph interaction, and the e–ph coupling constant,

λ ³⁸:

$$T_c = \frac{\Theta}{1.45} \exp\left(\frac{-1.04(1+\lambda)}{\lambda - \mu^*(1+0.62\lambda)}\right) \quad (3)$$

where the dimensionless constant μ^* accounts for the Coulomb repulsion, often referred as the Morel–Anderson pseudopotential³⁹. This formula is valid also for medium-coupling superconductors ($0.5 < \lambda < 1$). For Θ we consider the value corresponding to the zone-center optical phonon frequency $\omega_o = 9.2$ meV, as calculated by Kim et al.⁹, which is the frequency with the largest contribution to the e-ph coupling. With $\Theta = 106.2$ K, the experimental value of $\lambda = 0.58$, and $\mu^* = 0.1$, the estimated critical temperature from Eq. (3) is $T_c = 1.83$ K, in good agreement with the experimental value found with LT-STM.

When the McMillan formula is used for BCS superconductors with a cubic monoatomic lattice, Θ is often identified with the Debye temperature. A weak point of this approximation is that the Debye temperature is obtained from a fit of the specific heat, where the phonon degrees of freedom have all the same weight, whereas the corresponding contributions to the electron–phonon coupling are generally very different, with a possible dominant role of some specific phonons, as argued above. For a polyatomic crystal-like PdTe₂ it is nevertheless interesting to estimate the effective vertical component of the mean-square displacement in the definition of $2W(T) = k_{iz}^2 \langle u_z^2 \rangle_T$. By fitting the theoretical phonon branches of 1T-PdTe₂ calculated by Kim et al.⁹ with a dynamical model described in the Supplementary Note 8, where the three acoustic branches are treated in the Debye approximation (linear dispersion) and the six acoustic branches in the Einstein approximation (constant frequencies), the mean-square displacement in the normal direction and the high-temperature limit is found to be

$$\langle u_z^2 \rangle_T \cong \frac{k_B T}{\bar{f}} = 4.67 \cdot 10^{-5} \text{amu}^{-1} \text{meV}^{-2} k_B T \quad (4)$$

where $\bar{f} \equiv \overline{M\bar{\omega}^2}$ is the force constant of a single oscillator of mass \bar{M} and frequency $\bar{\omega}$. The above calculated mean-square displacement agrees well with the experimental value in the high-T limit:

$$\langle u_z^2 \rangle_T \cong \frac{2W(T)}{k_{iz}^2} = 4.47 \cdot 10^{-5} \text{amu}^{-1} \text{meV}^{-2} k_B T \quad (5)$$

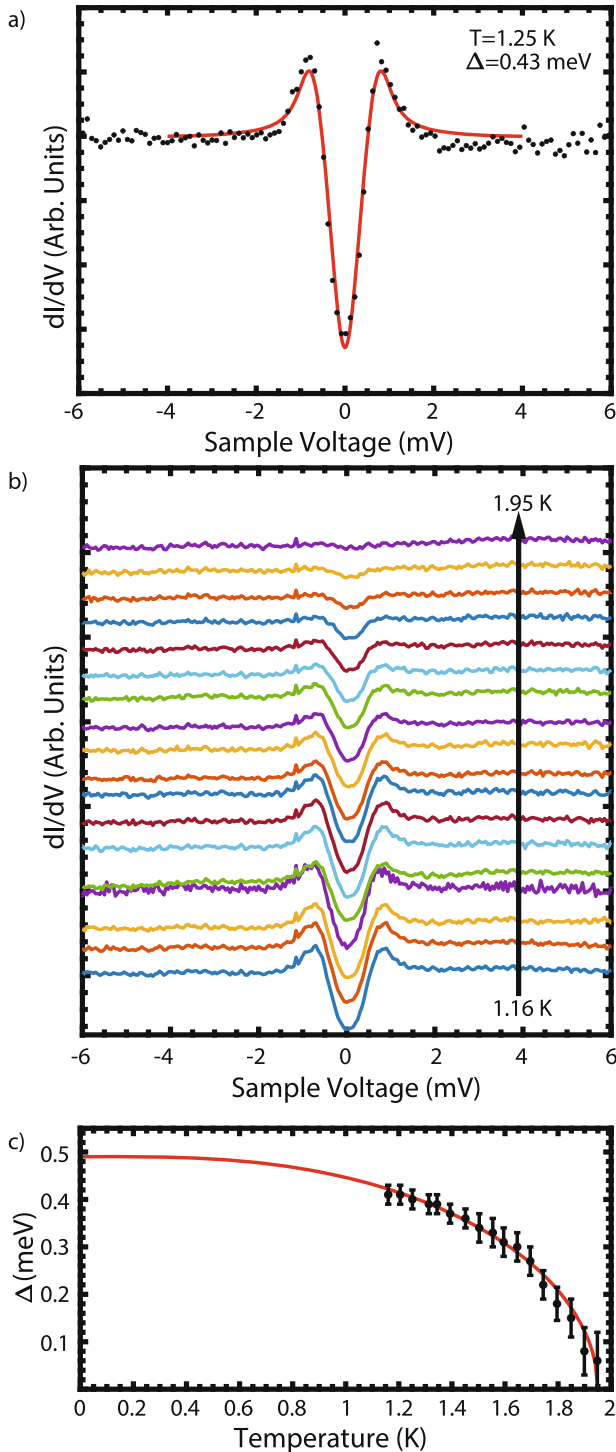


Fig. 3 Characterization of the superconducting gap by STS. **a** Representative dI/dV differential conductance spectrum of the 1T-PdTe₂ surface at 1.25 K, showing the characteristic superconducting gap in the absence of external magnetic field (black dots). **b** Normalized dI/dV spectra with varying temperatures from 1.16 to 1.95 K. **c** Evolution of the superconducting energy gap (Δ) with the temperature (black dots). The red lines in **(a)** and **(c)** represent the fit to the equation for a medium-coupling BCS superconductor³⁰.

A smaller experimental value indicates that the effective mean-square displacement of the surface-charge density, as given by HAS, is less than the one expected when the electrons move together with the atoms, as in the classical two-body collision

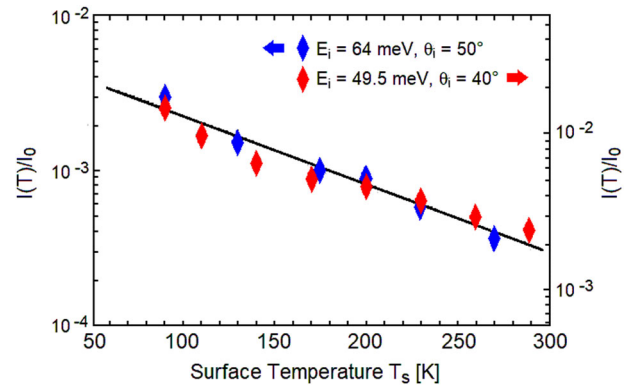


Fig. 4 E-ph coupling determination by the thermal attenuation of the He specular peak from PdTe₂. Thermal attenuation of He-specular intensity of 1T-PdTe₂ measured along $\overline{\Gamma M}$ at two different incident energies E_i and angles θ_i . Note the shifted log scale for the two sets of data, so as to have a single average slope for all data and an average $\lambda = 0.58 \pm 0.05$.

model. Such a difference, as long as significant, is indicative of an appreciable e-ph coupling.

Following Kim et al.⁹ argument, due to the saddle-point van Hove singularity near the Fermi-level, there is a specific phonon (e.g., O₂) giving a dominant e-ph interaction. We can identify such phonon with the above oscillator, whose $\overline{f}^{-1} = 4.47 \cdot 10^{-5} \text{ amu}^{-1} \text{ meV}^{-2}$ reproduces the experimental mean-square displacement. Since phonon dispersion curves are quite flat along the zone boundaries \overline{MK}^9 , zone-boundary phonons count more than those near the zone center. Thus, we search in Kim et al.⁹ phonon dispersion curve for the zone-boundary phonon whose combination $(\overline{M}, \overline{\omega})$ better fits the above \overline{f}^{-1} . The zone boundary LA phonon, having $\overline{M} \cong 2M_{\text{Te}} = 255.2 \text{ amu}$, $\overline{\omega} \cong 9.5 \text{ meV}$ ($\overline{f}^{-1} = 4.34 \cdot 10^{-5} \text{ amu}^{-1} \text{ meV}^{-2}$) clearly fits the experiment far better than any other zone-boundary phonon⁹. Note that this energy value is also close to that of the zone-center optical mode O₂ at 9.2 meV, which has the largest e-ph interaction⁹. Actually, the dip observed on the O₂ dispersion in approaching Γ (considered a signature of strong e-ph interaction), also affects the LA mode at the zone boundary, suggesting that also this mode should largely contribute to λ . While the O₂ modes around Γ couple at the Fermi-level to the saddle electronic states surrounding the six M points via intra-saddle ($\Delta k_{\parallel} \approx 0$) transitions, the M-point acoustic modes can couple to inter-saddle transitions between adjacent M-points, similarly to the intervalley coupling at the origin of Kelly-Falicov multivalley charge density waves (CDWs) in semiconductor surface quantum wells⁴⁰.

Therefore, in order to explain the origin of the e-ph coupling in PdTe₂, we consider the intervalley transitions, involving the zone-boundary LA phonons, in addition to intravalley transitions coming from a single cone, which involve the few zone-center O_{1,2} phonons. We suggest that the former mechanism is the dominant one for the large contribution of the zone-boundary phonons to the Eliashberg functions⁹ and for spin selection rules (diametric transitions in a Dirac cone reverse the spin). Topological states are involved in both cases. In general phonon-induced diametric intra-valley transitions between topological states requiring a spin-flip are only weakly allowed by the spin-orbit term, whereas there is no such selection for inter-valley transitions between equal-spin valleys. This conclusion is supported also by the ARPES data by Liu et al.⁴¹ showing at the Fermi level three intense spots β at about the midpoints between Γ and K, and equivalently three weak spots (β') between Γ and K'. These features correspond to the band 2 in Jan and Skriver LMTO calculations⁴² that cuts the Fermi level at $\Gamma K/2$ ($k_z = 0$) in Liu et al. band structure calculations) and evolves to a Dirac cone at AH/2

($k_z = \pi/c$) of the 3D BZ (see also Bahramy et al.³⁵ calculations). Kim et al.⁹ also note that a van Hove singularity of the electronic DOS just above the Fermi level at the M and M' points plays an important role in the electron–phonon interaction. On the basis of these ARPES indications, the major contribution to the e-ph coupling constant λ is very likely to be associated with phonon-induced intervalley $\beta - \beta$ or $\beta' - \beta'$ transitions involving states near the AH/2 points of equal spin. These transitions require phonons near the M point for being β about the mid-point of ΓK (and similarly β' of $\Gamma K'$), as well as the transitions between neighboring saddles M and M' suggested by Kim et al. analysis⁹.

In conclusion, we have determined experimentally the electron–phonon interaction for the superconductor 1T-PdTe₂ from the temperature dependence of Helium atom reflectivity. The mass-enhancement factor obtained in this way, $\lambda = 0.58 \pm 0.03$, agrees well with the theoretical value reported by Kim et al.⁹ ($\lambda = 0.53$) and yields, via McMillan's formula, a superconductivity critical temperature $T_c = 1.83$ K, in good agreement with the experimental result found by STS experiments, $T_c = (1.95 \pm 0.03)$ K, as well as with Kim et al. value at zero pressure ($T_c = 1.79$ K). The pressure dependence of T_c should be reflected in that of λ , via the shift of electronic states at the Fermi level and the anharmonic change of phonon frequencies. Kim et al. predict that van Hove singularities, held responsible for a comparatively large λ , get closer to the Fermi level with pressure⁹, while Xiao et al.³¹ predict a decrease of λ for increasing pressure. On the experimental side, Leng et al.³³ find an increase of T_c with pressure up to 1.91 GPa followed by a decrease at larger pressures. Indeed, by inserting Eq. (4) into Eq. (2), so as to obtain

$$\lambda = \frac{\pi\phi}{2n_s a_c \bar{f}}, \quad (6)$$

it appears that pressure may have two opposite effects: λ can either decrease as an effect of the effective force constant stiffening or increase due to the surface unit cell contraction (the rest remaining approximately unchanged). This would indicate that at low pressure the linear decrease of the surface area dominates over the incipient linear increase of the effective force constant, until the latter, due to the intrinsic nonlinearity of anharmonicity, gets more important.

The e-ph coupling in the isostructural 1T-PtTe₂ has been found to be substantially smaller ($\lambda = 0.38$)²⁵. The connection between the mass-enhancement factor λ and the phonon structure, via the HAS Debye–Waller exponent, allows to guess which phonons are more strongly coupled, in qualitative agreement with a recent first-principle analysis⁹. The differences in the phonon structure with the isostructural PtTe₂ lead to a stronger e-ph coupling in 1T-PdTe₂, which together with the presence of a van Hove singularity near the Fermi level, trigger superconductivity in 1T-PdTe₂. Very recently, however, Liu et al.⁴³ have reported that 4ML- and 6ML-PdTe₂ films deposited on SrTiO₃ exhibit a new type (type-II) Ising superconductivity, occurring in 2D centrosymmetric materials, with $T_c = 0.7015$ K and 0.7347 K, respectively, and a critical magnetic field parallel to the surface up to seven times the Pauli limit. In this case the role of e-ph coupling in pairing may be modest as compared to that of correlation, and the electrons involved at the Fermi level are concentrated at wavevectors around the G point. The actual role of the e-ph interaction could be assessed from HAS measurements of λ for the 6ML- and 4ML-films, where the slope of the DW exponent in Eq. (2) should decrease with thickness, similarly to what observed in thin metal films⁴⁴. Note that Eq. (2) is the 2D version of the general form for any dimension derived in⁴⁵, and that the saturation number n_s is < 4 , so that λ for the 4ML and 6ML films should be directly proportional to the observed DW slopes.

Furthermore, our analysis suggests that the topological states of a single cone play a negligible role in e-ph interaction and superconductivity, whereas the intervalley coupling, involving

topological states near zone boundaries, does the main job, as also found in recent results on Bi₂Se₃, Bi₂Se₂Te, and Bi₂Te₃⁴⁶. In the first two materials, where surface quantum-well bands cross the Fermi surface, the Kelly–Falicov intervalley e-ph interaction can support CDWs. HAS diffraction and inelastic spectra show, respectively, clear signatures of CDWs and of their collective excitations, which are hardly accessible to another current, less surface-sensitive probes. Similar HAS results have been reported for Sb(111), solving a long-debated question about the occurrence of a CDW in this surface⁴⁴. Considering that also several layered transition metal chalcogenides exhibit CDWs, either competitive or cooperative with superconductivity, HAS qualified as a valuable probe for future investigations of structural and e-ph properties in this important class of materials. A recent discussion on the role and results of HAS spectroscopy in the study of electron–phonon interaction in layered TMDs with an interplay between superconductivity and CDWs (e.g., 1T-TaS₂, 2H-TaSe₂, and 2H-NbSe₂) is found in ref. ⁴⁷. We finally note that the present set-ups of HAS spectrometers do not permit measurements under pressure, since at least a micrometric portion of the surface should be accessible, i.e., exposed to vacuum. This is however a challenge for the future, in view of the valuable information which could be collected for materials of great technological importance.

METHODS

Crystal growth

Single crystals of 1T-PdTe₂ were prepared by the slow cooling method as described elsewhere⁴⁸. Stoichiometric mixtures of high purity elements Pd sheet (3N) and Te ingots (7N) were melted at 900 °C for 24 h and slowly cooled to 450 °C in an evacuated quartz tube. The as-grown crystal was cleaved along the basal plane, with a shiny mirror-like surface. The stoichiometry and the structure of 1T-PdTe₂ single crystals were examined by means of a Bruker-D2 PHASER X-ray diffractometer using Cu-K α radiation and an energy-dispersive X-ray spectroscopy (EDX) (see Supplementary Figs. 1 and 2 and Supplementary Note 1).

HAS measurements

The 1T-PdTe₂ clean surface was prepared by flash-annealing in ultra-high vacuum (UHV), after crystal exfoliation. The UHV chamber has a base pressure of $\sim 9 \times 10^{-10}$ mbar. The experiments were performed with the thermal energy atomic and molecular scattering (TEAMS) apparatus⁴⁹. The He atom beam is produced by a free expansion of helium gas through a 30 μ m nozzle. The incident beam energy can be varied between 20 and 150 meV by regulating the nozzle temperature. In this apparatus, a mobile detector allows to measure the diffraction peaks for a spherical sector of 200° in-plane and $\pm 15^\circ$ out-of-plane and to measure the direct beam intensity. The manipulator enables sample positioning and orientation with 5 degrees of freedom. The sample can be moved in the X, Y and Z directions, rotated in the X-Y plane and changed the azimuthal angle (ϕ), which determines the incidence direction with respect to the lattice vector. The sample can be heated by electronic bombardment or cooled with liquid nitrogen (the lowest temperature obtainable in the HAS set-up is 90 K). The crystal temperature is measured by K-type thermocouple spot-welded to the sample holder.

STM/STS measurements

STM measurements were carried out in a custom-designed UHV chamber equipped with LT-STM, working at 1.25 K. In this system, it is possible to apply a ± 3 T magnetic field perpendicular to the sample. The sample was applied in situ, keeping the base pressure during the experiments at 8×10^{-10} mbar. All STM images were taken in constant-current mode and the differential conductance (dI/dV) spectra were acquired using a lock-in amplifier ($f = 763$ Hz, $V_{pp} = 100$ μ V). The WsXM and Gwyddion software were used to process the STM data^{50,51}.

DATA AVAILABILITY

The data supporting the findings of this work are available from the corresponding author upon reasonable request.

Received: 10 August 2020; Accepted: 22 January 2021;

Published online: 23 February 2021

REFERENCES

- Wang, Q. H., Kalantar-Zadeh, K., Kis, A., Coleman, J. N. & Strano, M. S. Electronics and optoelectronics of two-dimensional transition metal dichalcogenides. *Nat. Nanotechnol.* **7**, 699 (2012).
- Lv, R. et al. Transition metal dichalcogenides and beyond: synthesis, properties, and applications of single- and few-layer nanosheets. *Acc. Chem. Res.* **48**, 56–64 (2014).
- Jariwala, D., Sangwan, V. K., Lauhon, L. J., Marks, T. J. & Hersam, M. C. Emerging device applications for semiconducting two-dimensional transition metal dichalcogenides. *ACS Nano* **8**, 1102–1120 (2014).
- Mak, K. F. & Shan, J. Photonics and optoelectronics of 2D semiconductor transition metal dichalcogenides. *Nat. Photonics* **10**, 216 (2016).
- Pető, J. et al. Moderate strain induced indirect bandgap and conduction electrons in MoS₂ single layers. *NPJ 2D Mater. Appl.* **3**, 1–6 (2019).
- Subramanian, S. et al. Tuning transport across MoS₂/graphene interfaces via as-grown lateral heterostructures. *NPJ 2D Mater. Appl.* **4**, 1–5 (2020).
- Yan, L. et al. Identification of topological surface state in PdTe₂ superconductor by angle-resolved photoemission spectroscopy. *Chin. Phys. Lett.* **32**, 067303 (2015).
- Das, S. et al. Conventional superconductivity in the type-II Dirac semimetal PdTe₂. *Phys. Rev. B* **97**, 014523 (2018).
- Kim, K. et al. Importance of the van Hove singularity in superconducting PdTe₂. *Phys. Rev. B* **97**, 165102 (2018).
- Teknowijoyo, S. et al. Nodeless superconductivity in the type-II Dirac semimetal PdTe₂: London penetration depth and pairing-symmetry analysis. *Phys. Rev. B* **98**, 024508 (2018).
- Noh, H.-J. et al. Experimental realization of type-II Dirac fermions in a PdTe₂ superconductor. *Phys. Rev. Lett.* **119**, 016401 (2017).
- Clark, O. J. et al. Fermiology and superconductivity of topological surface states in PdTe₂. *Phys. Rev. Lett.* **120**, 156401 (2018).
- Leng, H., Paulsen, C., Huang, Y. & De Visser, A. Type-I superconductivity in the Dirac semimetal PdTe₂. *Phys. Rev. B* **96**, 220506 (2017).
- Salis, M. V., Rodière, P., Leng, H., Huang, Y. K. & de Visser, A. Penetration depth study of the type-I superconductor PdTe₂. *J. Phys.: Condens. Matter* **30**, 505602 (2018).
- Sirohi, A. et al. Mixed type I and type II superconductivity due to intrinsic electronic inhomogeneities in the type II Dirac semimetal PdTe₂. *J. Phys.: Condens. Matter* **31**, 085701 (2019).
- Fariás, D. & Rieder, K.-H. Atomic beam diffraction from solid surfaces. *Rep. Prog. Phys.* **61**, 1575 (1998).
- Manson, J., Benedek, G. & Miret-Artés, S. Electron-phonon coupling strength at metal surfaces directly determined from the helium atom scattering Debye-Waller factor. *J. Phys. Chem. Lett.* **7**, 1016–1021 (2016).
- Manson, J., Benedek, G. & Miret-Artés, S. Correction to electron-phonon coupling strength at metal surfaces directly determined from the helium atom scattering Debye-Waller factor. *J. Phys. Chem. Lett.* **7**, 1691–1691 (2016).
- Benedek, G., Miret-Artés, S., Toennies, J. P. & Manson, J. R. The electron-phonon coupling constant of metallic overlayers from specular He-atom scattering. *J. Phys. Chem. Lett.* **9**, 76 (2018).
- Tamtögl, A. et al. Electron-phonon coupling and surface Debye temperature of Bi₂Te₃(111) from helium atom scattering. *Phys. Rev. B* **95**, 195401 (2017).
- Anemone, G., Taleb, A. A., Benedek, G., Castellanos-Gomez, A. & Fariás, D. Electron-phonon coupling constant of 2H-MoS₂ (0001) from helium-atom scattering. *J. Phys. Chem. C* **123**, 3682–3686 (2019).
- Finlayson, T., Reichardt, W. & Smith, H. Lattice dynamics of layered-structure compounds: PdTe₂. *Phys. Rev. B* **33**, 2473 (1986).
- Kjekshus, A. & Grønvdal, F. High temperature X-ray study of the thermal expansion of PtS₂, PtSe₂, PtTe₂ and PdTe₂. *Acta Chem. Scand.* **13**, 1767–1774 (1959).
- Lyons, A., Schleich, D. & Wold, A. Crystal growth and characterization of PdTe₂. *Mater. Res. Bull.* **11**, 1155–1159 (1976).
- Anemone, G. et al. Experimental determination of surface thermal expansion and electron-phonon coupling constant of 1T-PtTe₂. *2D Materials* **7**, 025007 (2020).
- Liu, C. et al. Two-dimensional superconductivity and topological states in PdTe₂ thin films. *Phys. Rev. Mater.* **2**, 094001 (2018).
- Furuseth, S., Selte, K. & Kjekshus, A. Redetermined crystal structures of NiTe₂, PdTe₂, PtS₂, PtSe₂ and PtTe₂. *Acta Chem. Scand.* **19**, 257 (1965).
- Ryan, G. W. & Sheils, W. L. Electronic states and surface structure of PdTe₂ as probed by scanning tunneling microscopy and photoemission spectroscopy. *Phys. Rev. B* **61**, 8526–8530 (2000).
- Hooda, M. & Yadav, C. Electronic transport properties of intermediately coupled superconductors: PdTe₂ and Cu_{0.04}PdTe₂. *EPL* **121**, 17001 (2018).
- Gross, F. et al. Anomalous temperature dependence of the magnetic field penetration depth in superconducting UBe₁₃. *Z. Phys. B Condens. Matter.* **64**, 175–188 (1986).
- Xiao, R. et al. Manipulation of type-I and type-II Dirac points in PdTe₂ superconductor by external pressure. *Phys. Rev. B* **96**, 075101 (2017).
- Guggenheim, J., Hulliger, F. & Müller, J. PdTe₂, a superconductor with Cd₂ structure. *Helv Phys Acta* **34**, 408–410 (1961).
- Leng, H. et al. Superconductivity under pressure in the Dirac semimetal PdTe₂. *J. Condens. Matter Phys.* **32**, 025603 (2019).
- Rasmussen, F. A. & Thygesen, K. S. Computational 2D materials database: electronic structure of transition-metal dichalcogenides and oxides. *J. Phys. Chem. C* **119**, 13169–13183 (2015).
- Bahramy, M. et al. Ubiquitous formation of bulk Dirac cones and topological surface states from a single orbital manifold in transition-metal dichalcogenides. *Nat. Mater.* **17**, 21 (2018).
- McMillan, W. L. Transition temperature of strong-coupled superconductors. *Phys. Rev.* **167**, 331–344 (1968).
- Phan, D. & Chubukov, A. V. Kohn-Luttinger correction to T_c in a phonon superconductor. *Phys. Rev. B* **101**, 024503 (2020).
- Bardeen, J. C. L. & JR, S. Theory of superconductivity. *Phys. Rev.* **108**, 5 (1957).
- Morel, P. & Anderson, P. Calculation of the superconducting state parameters with retarded electron-phonon interaction. *Phys. Rev.* **125**, 1263 (1962).
- Kelly, M. & Falicov, L. Optical properties of charge-density-wave ground states for inversion layers in many-valley semiconductors. *Phys. Rev. B* **15**, 1983 (1977).
- Yan, L. et al. Electronic structure of transition metal dichalcogenides PdTe₂ and Cu_{0.05}PdTe₂ superconductors obtained by angle-resolved photoemission spectroscopy. *Chin. Phys. B* **24**, 067401 (2015).
- Jan, J.-P. & Skriver, H. L. Relativistic bandstructure and Fermi surface of PdTe₂ by the LMTO method. *J. Phys. F: Met. Phys.* **7**, 1719 (1977).
- Liu, Y. et al. Type-II Ising superconductivity and anomalous metallic state in macro-size ambient-stable ultrathin crystalline films. *Nano Lett.* **20**, 5728–5734 (2020).
- Tamtögl, A. et al. Statics and dynamics of multivalley charge density waves in Sb (111). *npj Quantum Mater.* **4**, 1–7 (2019).
- Benedek, G., Manson, J. R. & Miret-Artés, S. The electron-phonon interaction of low-dimensional and multi-dimensional materials from He atom scattering. *Adv. Mater.* **32**, 2002072 (2020).
- Benedek, G. et al. Origin of the electron-phonon interaction of topological semimetal surfaces measured with helium atom scattering. *J. Phys. Chem. Lett.* **11**, 1927–1933 (2020).
- Benedek, G. et al. Measuring the electron-phonon interaction in two-dimensional superconductors with He-atom scattering. *Cond. Matter* **5**, 79 (2020).
- D'Olimpio, G. et al. PdTe₂ transition-metal dichalcogenide: chemical reactivity, thermal stability, and device implementation. *Adv. Funct. Mater.* **30**, 1906556 (2019).
- Nieto, P., Barredo, D., Fariás, D. & Miranda, R. In-plane and out-of-plane diffusion of H₂ from Ru (001). *J. Phys. Chem. A* **115**, 7283–7290 (2011).
- Horcas, I. et al. WsXM: a software for scanning probe microscopy and a tool for nanotechnology. *Rev. Sci. Instrum.* **78**, 013705 (2007).
- Nečas, D. & Klapetek, P. Gwyddion: an open-source software for SPM data analysis. *Cent. Eur. J. Phys.* **10**, 181–188 (2012).

ACKNOWLEDGEMENTS

Work partially supported by the Ministerio de Economía y Competitividad (MINECO) projects MAT2015-65356-C3-3-R and FIS2015-67367 C2-1-P, the Ministerio de Ciencia, Innovación y Universidades projects PGC2018-093291-B-I00, PGC2018-097028-A-I00, PGC2018-098613-B-C21 and PID2019-109525RB-I00 and the Comunidad de Madrid (CM) projects Nanomag COST-CM/P2018/NMAT-4321 and NMAT2D-CM P2018/NMT-4511. We acknowledge financial support from the Spanish Ministry of Science and Innovation, through project PID2019-109525RB-I00 and the "María de Maeztu" Programme for Units of Excellence in R&D (CEX2018-000805-M). IMDEA Nanociencia acknowledges support from the "Severo Ochoa" Programme for Centres of Excellence in R&D (MINECO, Grant SEV-2016-0686). M.G. has received financial support through the Postdoctoral Junior Leader Fellowship Programme from "la Caixa" Banking Foundation.

AUTHOR CONTRIBUTIONS

D.F. and R.M. supervised the project. G.A. and A.A.T. carried out the HAS measurements. P.C.A., M.G., and G.A. performed the STM/STS measurements. C.N.K., C.S.L., and A.P. grew the PdTe₂ samples and made the XRD characterization. G.B.

performed and wrote the theoretical analysis. G.A., G.B., D.F., and R.M. conducted the HAS data analysis. P.C.A., M.G., F.C., A.V.P., and R.M. conducted the STM/STS analysis. M.G. contributed to the writing of the results. G.A. wrote the paper with input from all the authors. All authors discussed the results and contributed to the final manuscript.

COMPETING INTERESTS

The authors declare no competing interests.

ADDITIONAL INFORMATION

Supplementary information The online version contains supplementary material available at <https://doi.org/10.1038/s41699-021-00204-5>.

Correspondence and requests for materials should be addressed to G.A.

Reprints and permission information is available at <http://www.nature.com/reprints>

Publisher's note Springer Nature remains neutral with regard to jurisdictional claims in published maps and institutional affiliations.



Open Access This article is licensed under a Creative Commons Attribution 4.0 International License, which permits use, sharing, adaptation, distribution and reproduction in any medium or format, as long as you give appropriate credit to the original author(s) and the source, provide a link to the Creative Commons license, and indicate if changes were made. The images or other third party material in this article are included in the article's Creative Commons license, unless indicated otherwise in a credit line to the material. If material is not included in the article's Creative Commons license and your intended use is not permitted by statutory regulation or exceeds the permitted use, you will need to obtain permission directly from the copyright holder. To view a copy of this license, visit <http://creativecommons.org/licenses/by/4.0/>.

© The Author(s) 2021